Eur Biophys J (1994) 23:95–104

European Biophysics Journal

Vibrational mode analysis of 2-aminoadenine and its deuterated species from Raman and ultraviolet resonance Raman data

Z. Dhaouadi [1], M. Ghomi [1], P. Mojzes [2], P. Y. Turpin [3], L. Chinsky [3]

[1] Physique Théorique des Macromolécules Biologiques, UFR Santé-Médecine-Biologie Humaine, Université Paris XIII, 74 rue Marcel Cachin, F-93012 Bobigny Cedex, France
[2] Institute of Physics, Charles University, Ke Karlovu 5, 12116 Prague, Czech Republic
[3] Laboratoire de Physique et Chimie Biomoléculaires, CNRS URA 198, Institut Curie et Université Paris VI, 11 rue Pierre et Marie Curie, F-75231 Paris Cedex 05, France

Received: 15 July 1993 / Accepted in revised form: 10 January 1994

Abstract. Resonance Raman spectroscopy data of 2-aminoadenine and its deuterated species (C8-deuterated, N-deuterated and C8-, N-deuterated derivatives) in aqueous solution have been collected in the spectral region between 400 and 1800 cm^{-1}, by using ultraviolet excitation wavelengths (λ_{exc} = 222, 257 and 281 nm) located in the three main UV absorption bands corresponding to the strongly allowed electronic transitions of the molecule of interest. Moreover, a Raman spectrum has been recorded under off-resonance conditions with a visible excitation (λ_{exc} = 488 nm). In order to assign the 2-aminoadenine in-plane vibrational bands displayed in the RRS spectra, a normal coordinate analysis has been performed by means of an empirical internal valence force field. These calculations are based on our recent normal mode analysis of adenine and guanine nucleic bases and their deuterated species, which was based on the joint use of resonance Raman spectroscopy and neutron inelastic scattering data. In the 2-aminoadenine force field proposed here, the diagonal force constants have been directly transferred from those recently obtained for adenine (and from guanine as concerns the 2-amino group), the interaction force constants (off-diagonal) then being adjusted on the basis of the actual experimental data from 2-aminoadenine and its deuterated species. The current force field is also able to assign infrared and Raman data obtained by other authors from polycrystalline samples of the pure species.

Key words: Resonance Raman spectroscopy – Vibrational mode analysis – 2-Aminoadenine – Nucleic acids – Molecular force field

I. Introduction

2-aminoadenine (2,6-diaminopurine: $2NH_2A$) is a minor purine base whose biological significance was demonstrated some time ago by various investigators (Kirnos et al. 1977; Khudyakov et al. 1978). As compared to adenine (A), the C2-hydrogen atom is replaced in $2NH_2A$ by an amino-group (Fig. 1): such a change in a chemical function enables a third hydrogen bond between $2NH_2A$ and its complementary base (thymine T or uracil U) to be formed in the Watson-Crick base pairing model of double-helical nucleic acids. This additional hydrogen bond considerably increases the melting temperature of the helical duplex and makes it comparable to that of a guanine-cytosine (G-C) duplex (Gaffney et al. 1982). This property of $2NH_2A$ has given rise to a series of spectroscopic investigations on various compounds containing this purine base: conformational transitions of DNA double-helices containing $2NH_2A$-T (or $2NH_2A$-U) base pairs have been monitored by means of ^{31}P NMR (Howard et al. 1984), 2D ^1H NMR (Borah et al. 1985, 1986), circular dichroism (Gaffney et al. 1982; Howard et al. 1984; Borah et al. 1986; Vorlickowa et al. 1988), infrared (Howard et al. 1984; Taboury et al. 1984; Garriga et al. 1992) and ultraviolet resonance Raman (Mojzes et al. 1992) spectroscopies. Finally, the crystal structure of Z-DNA hexamers containing $2NH_2A$-T base pairs has been obtained at a 1.3 Å resolution (Coll et al. 1986) and X-ray diffraction patterns of poly($d2NH_2A$-dT) fibers at 98% relative humidity have also been recently studied (Alexeev et al. 1990).

A complete vibrational mode analysis of $2NH_2A$ and its associated nucleoside and nucleotide is necessary for a better assignment of the conformational marker modes observed in the vibrational spectra of oligo- and polynucleotides containing this purine base. Until now, only one paper has reported ab initio vibrational analysis of $2NH_2A$, based only on IR and Raman data of the pure polycrystalline species (Florian et al. 1992). No experimental data has yet been produced for the isotopic derivatives of this molecule: this lack of experimental data makes it difficult to reliably assign the molecular vibrational modes.

Here we report resonance Raman (RRS) and off-resonance Raman spectra of $2NH_2A$ and its deuterated spe-

Correspondence to: M. Ghomi

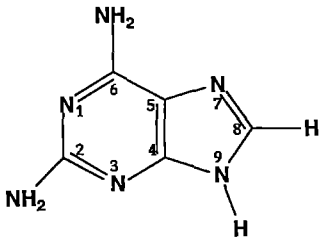

2-aminoadenine

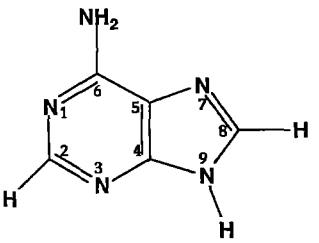

Adenine

Fig. 1. Chemical structure and atom numbering of adenine and 2-aminoadenine ($2NH_2A$) molecules

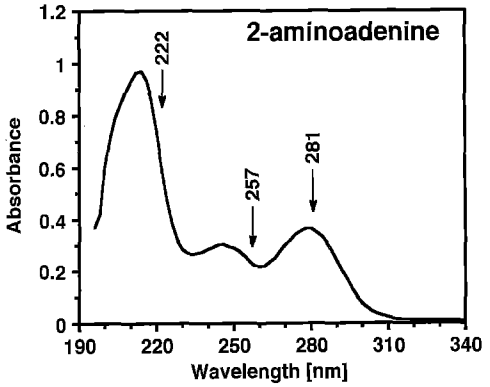

Fig. 2. Ultraviolet electronic absorption spectrum of $2NH_2A$. The positions of the three UV excitation wavelengths used to record RRS spectra are indicated by vertical arrows

cies, taken at various excitation wavelengths. A normal mode calculation has then been carried out, based on the observed vibrational modes. This vibrational analysis has been performed in the light of our recent empirical force field calculations based on the RRS and neutron inelastic scattering (NIS) spectra of adenine (Dhaouadi et al. 1993 a), guanine (Dhaouadi et al. 1993 b) and their deuterated derivatives.

II. Experimental

A. Materials

$2NH_2A$ of highest available purity was a generous gift from Dr. Antonin Holy (Institute of Organic Chemistry, Czech Academy of Science). The deuterium exchange of nitrogen protons of nucleic acid bases is known to be nearly instantaneous (Livramento and Thomas 1974; Laigle et al. 1989). Thus, the N2-, N6- and N9-deuterated species ($2NH_2A$-d5) was prepared by simply dissolving polycrystalline $2NH_2A$ in D_2O (99.98%, Aldrich Chemical) at 25°C. In contrast, the deuterium exchange rate at the C8 position is almost negligible at room temperature. However, heating up to 80°C increases this rate by more than 3 orders of magnitude (Thomas and Livramento 1975). We have obtained a highly pure N2-, N6-, C8- and N9-deuterated species ($2NH_2A$-d6) by heating the $2NH_2A$-d5 species at 80°C for 20 h. Finally, the C8-deuterated species ($2NH_2A$-d1) was obtained by dissolving $2NH_2A$-d6 (crystallized from D_2O) in H_2O.

The solutions of $2NH_2A$-d1 (in H_2O) were kept in the refrigerator (4°C) to minimize the reverse slow isotopic exchange at the C8 site. Also, the corresponding Raman spectra were recorded at 4°C. All of the solutions were prepared for resonance Raman measurements at base concentrations of 1.6 mM in H_2O (D_2O) and adjusted to pH (pD) 7.0 with HCl (DCl). The base concentration for off-resonance Raman experiments was ca. 50 mM.

B. Raman spectra

In the present work, UV RRS spectra were recorded in the 400–1800 cm^{-1} range by using the 222 and 281 nm pulsed laser (Quantel Datachrom 5000 Nd-Yag and dye laser system) and 257 nm continuous (cw) laser excitation wavelengths (second harmonic of the 514.5 nm line of a Lexel Ar^+ mode-locked laser). This spectral range covers most of the modes arising from ring stretching and bending internal coordinates (and their couplings); the regions below 400 cm^{-1} and above 2500 cm^{-1}, mostly corresponding to out-of-plane and pure C-H and N-H stretching modes, respectively, are much less active in resonance Raman, especially in aqueous solutions. Off-resonance Raman spectra were recorded here in the same spectral range by using cw 488 nm excitation. However, the two ring in-plane bending modes located below 400 cm^{-1} and measured in the IR and 514 nm Raman spectra of the pure species in polycrystalline form (Florian et al. 1992) have been also used in our analysis.

The experimental setup has been previously described (Miskovsky et al. 1989). The Raman spectra presented in this paper are averages of 6 to 16 consecutive scans recorded at 1 cm^{-1} increments. The broad Raman scattering contributions from H_2O (D_2O) bending motions have been subtracted in the 1640 (1250) cm^{-1} region after peak intensity normalization on the large O-H (O-D) 3450 (2500) cm^{-1} stretching bands. The resulting spectra have then been smoothed either by the Savitsky-Golay method (1964) or by fast Fourier transform (Laigle et al. 1982).

To have an idea of the electronic transitions which are excited with the three UV laser wavelengths used in this paper, the electronic absorption spectrum of $2NH_2A$ in aqueous solution, recorded at room temperature on a VARIAN DMS 70 UV-visible spectrophotometer, is shown in Fig. 2. The Raman and RRS spectra of aqueous solutions of $2NH_2A$ are shown in Fig. 3. In the same manner, Raman and RRS spectra of the deuterated spe-

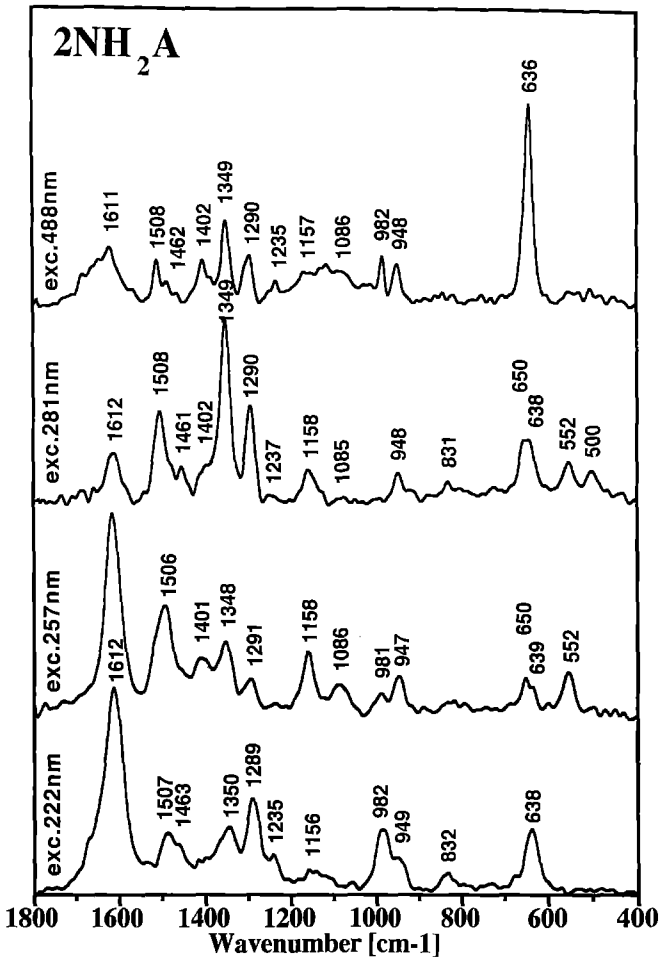

Fig. 3. Off- and on-resonance Raman spectra (taken at 4°C) from aqueous solutions of $2NH_2A$ in the spectral region between 1800 and 400 cm^{-1}. The excitation wavelengths (λ_{exc} = 222, 257, 281 and 488 nm) are indicated on each spectrum. See also Table 2

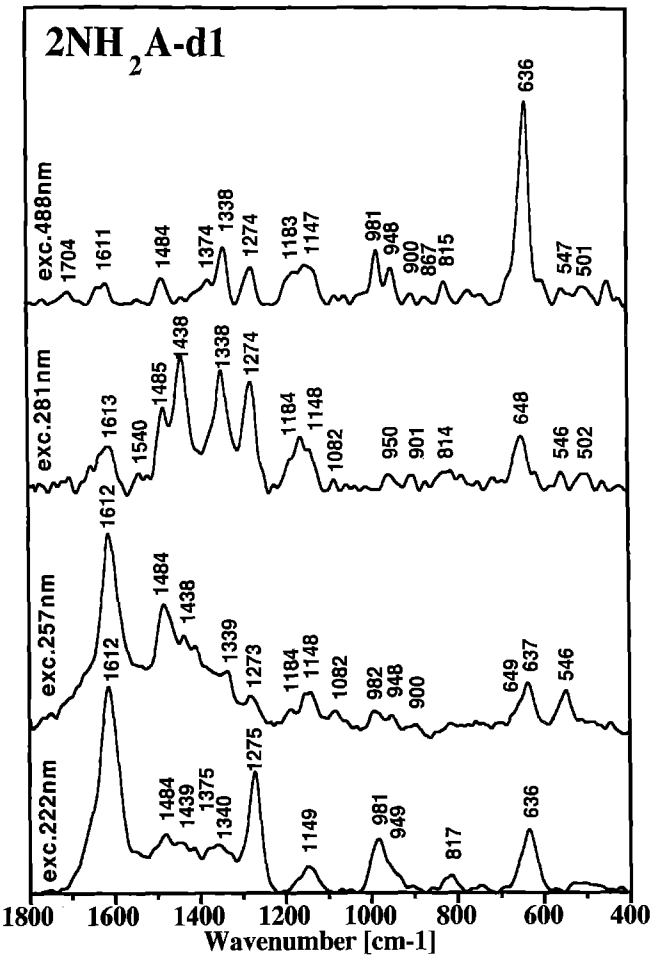

Fig. 4. Same as Fig. 3, but for $2NH_2A$-d1 (see also Table 3)

cies are shown in Fig. 4 ($2NH_2A$-d1), Fig. 5 ($2NH_2A$-d5), and Fig. 6 ($2NH_2A$-d6).

III. Normal mode calculations

A. Computational details

$2NH_2A$ base (Fig. 1) and deuterated species ($2NH_2A$-d1, $2NH_2A$-d5 and $2NH_2A$-d6) are supposed to be planar (C_S symmetry). 31 in-plane (2N-3) and 14 out-of-plane (N-3) vibrational modes are expected from these molecules. Only the in-plane motions have been considered in our current analysis of the vibrational modes actually observed in the Raman and RRS spectra. To simulate the molecular vibrations, 18 stretching and 27 angular bending internal coordinates have to be used, of which 14 are redundant. The 14 redundant internal valence coordinates have been removed by a diagonalisation procedure of the G-matrix (Gusoni and Zerbi 1968). The vibrational mode wavenumbers and atomic displacements were computed using a home-made calculation code (named BORNS for "BObigny Raman and Neutron Scatterings") developed within the framework of the Wilson GF-method (Wilson et al. 1955). All of the numerical computations were carried out on a SUN 4 sparc server.

B. Empirical harmonic internal valence force field of 2-aminoadenine

In the adenine in-plane valence force field reported in our previous papers based on NIS and RRS data (Dhaouadi et al. 1993a), the diagonal force constants were the same as Majoube's (1985), since he proposed very sound assignments from IR and Raman data of ^{15}N and D substituted species. Owing to the structural resemblance of adenine and $2NH_2A$ (Fig. 1), we have transferred, as they are, the adenine diagonal force constants to $2NH_2A$. In addition, the diagonal force constants of the C2-aminogroup have merely been transferred from those of guanine (Dhaouadi et al. 1993b) for the corresponding group of $2NH_2A$. Then, we have only refined some of the interaction (non-diagonal) force constants of A (and G for the 2-amino group) by a least-squares method, in using the following criterion: in each of the refinement cycles, only the force constants providing the most important

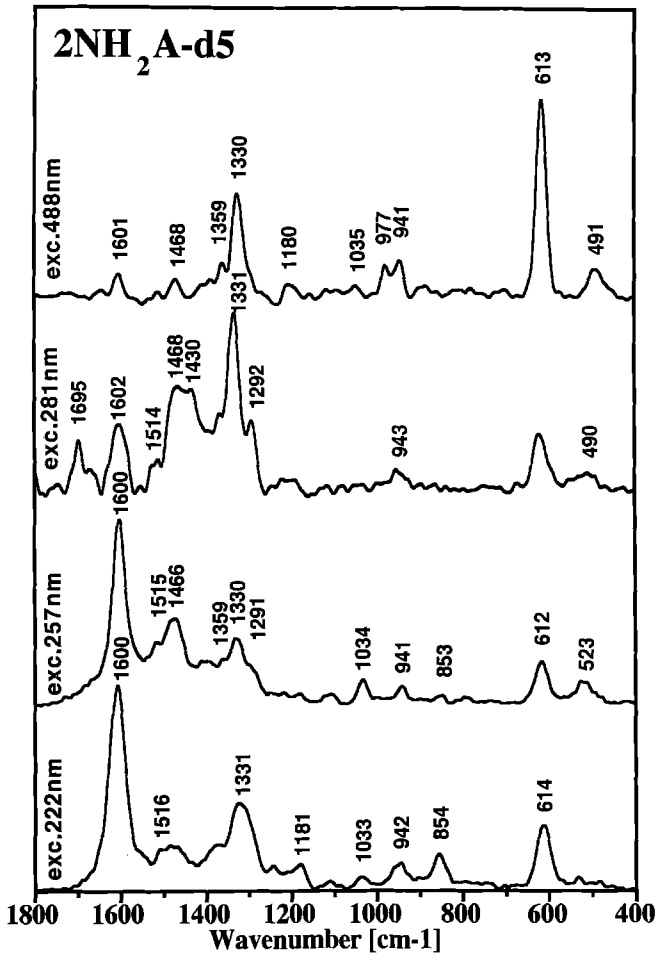

Fig. 5. Same as Fig. 3, but for $2NH_2A$-d5 (see also Table 4)

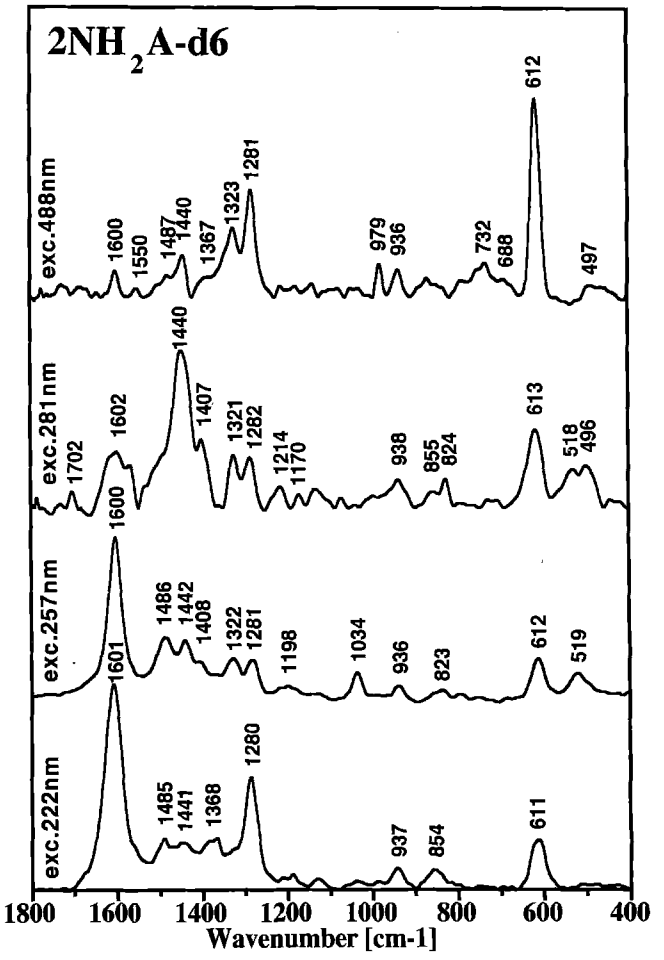

Fig. 6. Same as Fig. 3, but for $2NH_2A$-d6 (see also Table 5)

Jacobian matrix values (for pure and deuterated species) were selected and refined. From our previous experience, this refinement procedure for the non-diagonal force constants only is the most efficient way of fitting the calculated and observed frequencies and for simulating the isotopic shifts: attempts made in varying the diagonal force constants, even by significant amounts, only led to a few wavenumber changes of the vibrational modes, far too weak to correctly assign the actually observed wavenumbers of $2NH_2A$ and their isotopic shifts.

In Table 1, the interaction force constants of $2NH_2A$ are reported and compared to those of adenine (Dhaouadi et al. 1993a) and guanine (Dhaouadi et al. 1993b). Only 65 non-diagonal force constants (out of 77) have been adjusted by taking into account 80 (73 from our measurements plus 7 from IR and Raman data of polycrystalline samples (Florian et al. 1992)) vibrational mode wavenumbers observed in the spectra of $2NH_2A$ and deuterated species (Tables 2–5).

C. Calculated wavenumbers, assignments and normal mode representation

$2NH_2A$ and its deuterated derivatives provide 25 calculated in-plane vibrational modes below 1800 cm^{-1}. In this spectral region, the calculated and observed wavenumbers of the in-plane modes, and their assignments based on the Potential Energy Distribution (PED) matrix, have been reported in Tables 2 to 5 for the $2NH_2A$, $2NH_2A$-d1, $2NH_2A$-d5 and $2NH_2A$-d6 species, respectively. In Table 2 are also reported IR and Raman wavenumbers obtained from polycrystalline samples of the pure species and previously published (Florian et al. 1992). In Table 6 we show a selection of some of the most characteristic Raman modes of the pure species ($2NH_2A$) and their corresponding shifts calculated on isotopic substitutions. It is to be noted that the rule of additivity of the isotopic shifts (on progressive deuteration) proposed by Alix (1975) is qualitatively respected for some modes, but not for the complicated motions involving couplings between ring stretching and exocyclic hydrogen bending modes: this is likely to be due to the relative complexity of the molecule of interest. On the other hand, a direct comparison of the observed and/or calculated frequencies of adenine and $2NH_2A$ can be found elsewhere (Dhaouadi 1993), or can be made by referring to our previous paper on adenine (Dhaouadi et al. 1993a).

To help in the following discussion, the graphical representations of the calculated $2NH_2A$ vibrational modes located below 1800 cm^{-1} are presented in Fig. 7. For each vibrational mode the equilibrium structure and the

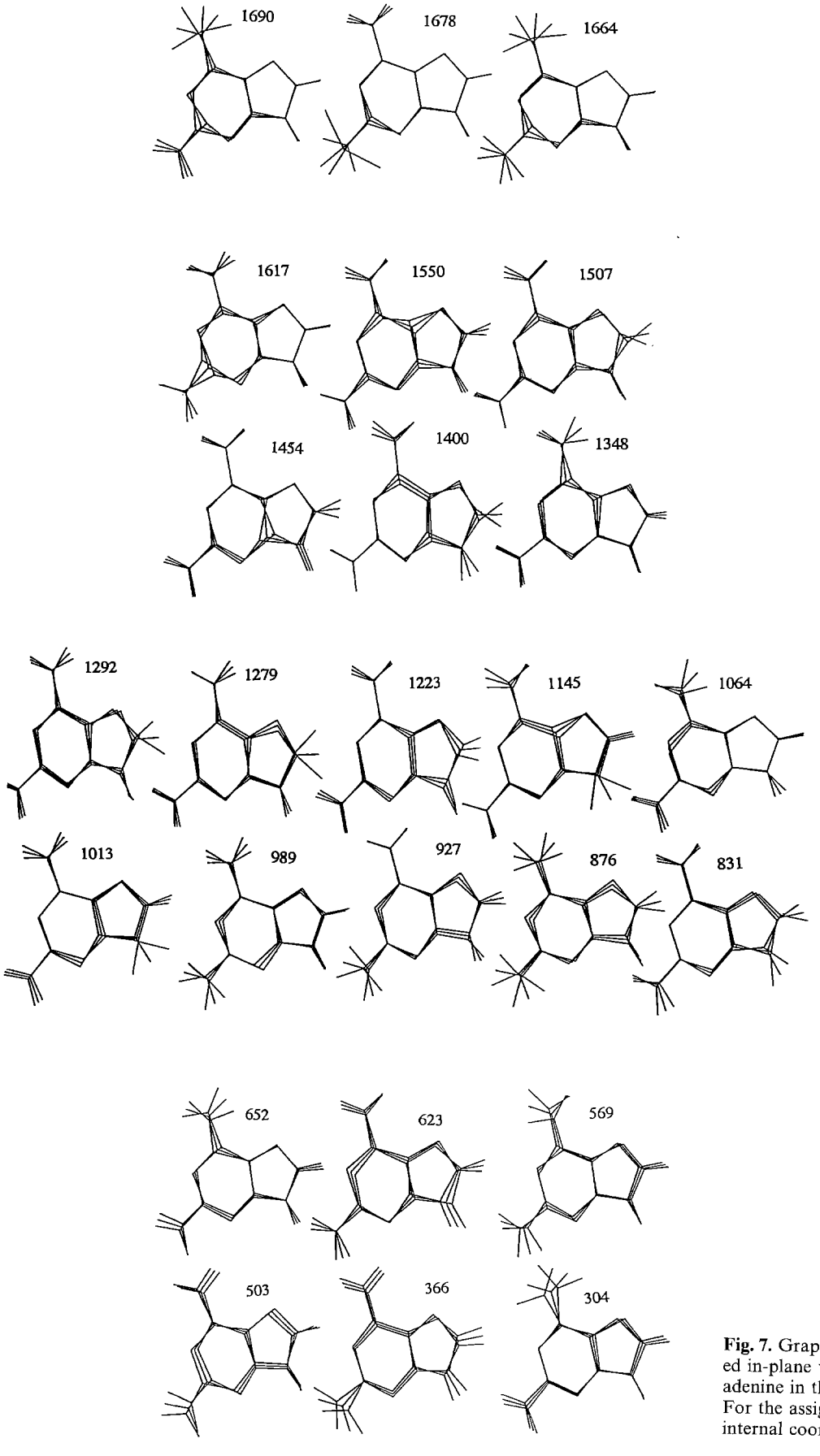

Fig. 7. Graphical representation of the calculated in-plane vibrational modes of 2-aminoadenine in the spectral region below 1800 cm^{-1}. For the assignment of these modes in terms of internal coordinates, see Table 2

most distorted configuration have been drawn on the same figure.

IV. Discussion

On the basis of the current normal mode analysis (Tables 2–5), we now want to discuss four distinct spectral regions associated with various categories of vibrational motions which give rise to some of the most intense bands experimentally observed; at the same time we review the recent assignments obtained from a quantum mechanical calculation at the STO-3G level (Florian et al. 1992), based on IR and Raman data obtained on the pure species only.

1800–1650 cm^{-1} spectral region

Three modes (1690, 1678 and 1664 cm^{-1}, see Table 2) are calculated in this spectral region. The first two mainly involve NH_2-scissoring motions in the 6- and 2-positions, respectively, while the last mode corresponds to their coupling (Fig. 7). Raman spectra generally provide only weak bands in this spectral region (Fig. 3). However, two bands at 1715 and 1661 cm^{-1} have been observed in the IR spectra of a polycrystalline sample, which are assignable to these vibrational motions.

1650–1340 cm^{-1} spectral region

Six vibrational modes have been calculated in this range. All of them are assigned to ring single- or double-bond stretching motions (some of them are slightly coupled with exocyclic hydrogen bendings), and all but one (1550 cm^{-1}) give rise to RRS, off-resonance Raman and IR bands. Among them, the mode calculated at 1617 cm^{-1} (and observed here at 1612 cm^{-1} in the Raman spectra of aqueous sample) mainly arises from pyrimidine ring stretching motions (Table 6). The relative intensity of this Raman band depends strongly on the excitation wavelength (Fig. 3). On the other hand, its wavenumber is completely insensitive to selective deuteration at the C8-position (Fig. 4 and Table 3). This experimental observation does not support the assignment recently made by Florian et al. (1992), who assumed for this mode an important contribution from imidazole ring vibrations, and especially N7=C8 bond-stretching motions. Our current Raman spectra show the insensitivity of this mode to C8 deuteration, in going from $2NH_2A$ to $2NH_2A$-d1, or from $2NH_2A$-d5 to $2NH_2A$-d6 (Tables 2 to 5): thus, this rules out possible contributions of N7=C8 bond-stretching motions in this vibrational mode.

Another intense RRS band observed here at 1508 cm^{-1} (and calculated at 1507 cm^{-1}), whose intensity varies significantly with the excitation wavelength, is mainly assigned to N7=C8 bond-stretching motions (Fig. 3 and Tables 2, 6). This is supported by an experimental 23 cm^{-1} wavenumber downshift upon C8-deuteration (Fig. 4 and Table 3). Again, the previous assignment made of this band by Florian et al. (1992) is in contradiction with the present experimental evidence. It should also be mentioned that our assignment of this mode resembles that of the intense adenine Raman mode observed at 1483 cm^{-1} (Dhaouadi et al. 1993a).

Finally, the intense RRS band observed here at 1349 cm^{-1} (and calculated at 1348 cm^{-1}) shows an evident resonance character (Figs. 3 and 7) and contains contributions from both the pyrimidine and imidazole moieties of the molecule, with strong bond-stretching characters (Table 2).

1300–800 cm^{-1} spectral region

The vibrational modes are calculated in this spectral region: all of them are mainly assigned to angular deforma-

Table 1. Non diagonal (interaction) valence force constants of $2NH_2A$ and its deuterated species. The values of these force constants are compared to those of adenine (A) (Dhaouadi et al. 1993a) and guanine (G) (Dhaouadi et al. 1993b) for the 2-aminogroup (in parentheses). Diagonal force constants (not shown here) were the same as those used in our previous calculations on adenine and guanine bases (see text). Units: Stretch-Stretch force constants: mdyn/Å; Bend-Bend force constants: mdyn. Å; Stretch-Bend force constans: mdyn. For atom numbering, see also Fig. 1

Interactions	Values	Interactions	Values
Stretch-Stretch		Stretch-Bend	
N9C8, C4N9	0.200 (0.200 A)	N9C8, C8N9H	0.500 (0.000 A)
N7C5, C4C5	0.200 (0.000 A)	N9C4, C4N9H	0.500 (0.270 A)
C4N3, C4C5	0.750 (0.350 A)	C8N7, N7C8H	0.550 (0.000 A)
C4C5, C6C5	0.750 (0.440 A)	N9C8, N9C8H	0.050 (0.760 A)
C6C5, N1C6	0.950 (0.650 A)	C6N6, C6N6H	−0.050 (0.000 A)
C6C5, N7C5	0.500 (−0.150 A)	C2N2, C2N2H	0.100 (0.350 G)
C4N3, C4N9	0.300 (0.200 A)	N9C8, N9C8N7	0.200 (0.000 A)
C6N6, C6C5	0.450 (0.750 A)	N9C8, N9C8C4	0.800 (0.800 A)
C8N7, C2N3	0.100 (−0.170 A)	C8N7, N9C8N7	0.250 (0.580 A)
C8N7, C4C5	0.400 (0.150 A)	C8N7, C8N7C5	0.200 (0.580 A)
C2N3, C4C5	0.200 (−0.150 A)	C4N9, C4N9C8	0.900 (0.900 A)
C8N7, C5N7	0.900 (0.900 A)	C4N9, N9C4C5	0.900 (0.900 A)
C8N7, C8N9	0.900 (0.900 A)	C4N9, N3C4N9	0.850 (0.550 A)
C8N7, C4N9	−0.400 (−0.710 A)	N7C5, N7C5C4	0.900 (0.000 A)
N3C2, N1C2	0.700 (0.500 A)	N7C5, C8N7C5	0.400 (0.750 A)
N3C2, N3C4	0.100 (0.250 A)	N7C5, N7C5C6	0.500 (0.750 A)
C6N6, N1C6	0.700 (0.801 A)	C5C6, C5C6N6	0.400 (0.200 A)
C5C4, C4N9	0.150 (0.150 A)	C5C6, N1C6C5	0.400 (0.200 A)
N9C4, C6C5	0.100 (0.150 A)	C5C6, N7C5C6	−0.300 (−0.300 A)
N1C2, C2N2	0.200 (0.450 G)	C5C6, C6C5C4	0.750 (0.200 A)
C2N2, C2N3	0.300 (0.450 G)	C5C4, N7C5C4	0.500 (0.000 A)
N1C6, N1C2	−0.200 (0.641 A)	C5C4, N9C4C5	0.500 (0.300 A)
N1C6, N3C2	−0.200 (0.150 A)	C5C4, C6C5C4	0.750 (0.750 A)
N1C6, N7N8	0.150 (0.220 A)	C5C4, N3C4C5	0.750 (0.300 A)
		C4N3, N3C4C5	0.900 (0.701 A)
		C4N3, C4N3C2	0.100 (0.701 A)
Bend-Bend		C4N3, N3C4N9	0.750 (0.550 A)
C4N9C8, C4N9H	−0.350 (−0.220 A)	C2N1, N3C2N1	0.200 (0.701 A)
C4N9C8, C8N9H	−0.150 (−0.220 A)	C2N1, C2N1C6	0.300 (0.701 A)
N9C8N7, N7C8H	−0.050 (−0.550 A)	C2N1, N1C2N2	0.300 (0.907 G)
N9C8N7, N9C8H	−0.550 (−0.550 A)	N3C2, N3C2N2	0.300 (0.907 G)
N1C6N6, C6N6H	−0.600 (0.250 A)	N3C2, C4N3C2	0.300 (0.750 A)
C5C6N6, C6N6H	0.200 (0.200 A)	N3C2, N3C2N1	0.100 (0.750 A)
N1C2N2, C2N2H	−0.150 (−0.05 G)	N1C6, N1C6N6	0.600 (0.780 A)
N3C2N2, C2N2H	−0.150 (−0.05 G)	N1C6, N1C6C5	0.600 (0.620 A)
HN6H, C6N6H	−0.010 (0.000 A)	N1C6, C2N1C6	0.300 (0.400 A)
HN2H, C2N2H	−0.005 (−0.013 A)	C6N6, N1C6N6	0.400 (0.901 A)
N1C6N6, N1C6C5	0.650 (0.390 A)	C6N6, C5C6N6	0.400 (0.901 A)
C5C6N6, N1C6C5	−0.100 (−0.100 A)	C2N2, N1C2N2	0.400 (0.000 G)
C5C6N6, N7C5C6	0.600 (−0.450 A)	C2N2, N3C2N2	0.400 (0.000 G)

Table 2. Comparison of experimental wavenumbers (cm^{-1}) (Raman spectra fom aqueous solutions obtained with the 488, 281, 257 and 222 nm excitation wavelengths) and calculated wavenumbers for $2NH_2A$ in-plane modes, in the spectral region below 1800 cm^{-1} (see also Fig. 3). The assignments are based on the internal coordinates for which the potential energy distribution (PED) is reported in % (PED contributions $\leq 7\%$ are not reported). Abbreviations: (vs): very strong, (s): strong, (m): medium, (w): weak, (sh): shoulder. IR and R stand for previously published polycrystalline infrared and Raman peaks (obtained with the 514.5 nm excitation wavelength), respectively (Florian et al. 1992)

Poly-crystal IR	R 514,5 nm	Solution R 488 nm	RRS 281 nm	RRS 257 nm	RRS 222 nm	Calc.	Assigments (PED)
1715						1690	H-N6-H scissoring (21%), C2N2 (17%), N1C6 (9%), C6N6H (8%)
	1680					1678	H-N2-H scissoring (47%), C2N2 (24%), C2N2H (21%)
1661	1667					1664	H-N6-H scissoring (23%), C2N2 (15%), C6N6 (8%)
1620	1614	1611 (m)	1612 (m)	1613 (s)	1612 (s)	1617	N3C2 (30%), C2N1 (25%)
						1550	C5C4 (22%), C6C5 (20%), C6N6 (9%)
1508	1510	1508 (m)	1508 (s)	1506 (sh)	1507 (m)	1507	C8N7 (26%), N9C8H (12%), C6N6 (9%), C6C5 (8%)
1445	1451	1462 (sh)	1461 (w)		1463 (sh)	1454	C4N3 (35%), C4N9 (24%)
1402	1400	1402 (w)	1402 (sh)	1401 (w)		1400	C8N7 (16%), C6N6 (16%), N9C8H (11%), C5C4 (10%)
1358	1355	1349 (s)	1349 (vs)	1348 (m)	1350 (m)	1348	N1C6 (31%), C6C5 (12%), N7C5 (11%), C5C6N6 (9%)
1286	1289	1290 (m)	1290 (s)	1291 (w)	1289 (s)	1292	N7C5 (17%), N7C8H (15%), N9C8 (14%), N9C8H (10%)
						1279	N9C8H (22%), N7C8H (15%), C8N7 (16%), N7C5 (11%), N1C6 (11%)
1244		1235 (w)	1237 (vw)		1235 (w)	1223	N9C8 (46%), C4N3 (11%)
1155	1169	1157 (sh)	1158 (m)	1158 (m)	1156 (vw)	1145	C4N9H (25%), C8N9H (16%), C6N6 (20%)
1092	1097	1086 (sh)	1085 (vw)	1086 (w)		1064	C6N6 (27%), C2N1 (18%), C6N6H (11%), C2N2 (10%)
1007	998					1013	C4N9H (29%), C8N9H (22%), C4N9 (17%), C2N2 (9%)
		982 (w)		981 (w)	982 (m)	989	C2N2H (22%), N3C2 (21%), C4N9 (8%)
937	940	948 (w)	948 (w)	947 (w)	949 (sh)	927	C2N2H (28%), N9C8 (10%), C5C4 (8%)
	890					876	C2N2H (23%), C6N6H (15%), C2N1 (8%)
843			831 (vw)		832 (vw)	831	C8N9H (16%), N7C5 (12%), C4N9C8 (10%), C8N7 (9%), N7C8H (8%)
658	659		650 (sh)	650 (w)		652	C5C6N6 (13%), C6N6 (11%), C2N1 (10%)
638	637	636 (vs)	638 (m)	639 (sh)	638 (m)	623	C4N9 (19%), N3C4C5 (11%), C6C5 (9%), C2N1C6 (8%), N3C2 (8%)
563	550		552 (w)	552 (w)		569	C6C5 (13%), C2N1C6 (10%), C6N6H (9%), N3C2N2 (9%)
507	508		500 (w)	500 (vw)		503	C4N3C2 (12%), N1C6C5 (11%), C5C6N6 (9%), C4N3 (9%), N1C6 (8%), N3C2N1 (8%)
366	376					366	N3C2N2 (14%), C6C5 (13%), N1C2N2 (12%), N3C4N9 (11%), N7C5C6 (10%)
	307					304	N1C6N6 (32%), C6N6H (17%), C5C6N6 (14%)

tions, especially those involving exocyclic hydrogens. This is also evident from the examination of Fig. 7. Experimentally, nine of them give spectral contributions in IR, off-resonance and resonance Raman spectra (see Table 2). The most intense RRS band observed in this region is located at 1290 cm^{-1} (Fig. 3); it is mainly assigned to NC8H angular bending motions and calculated at 1292 cm^{-1} (Table 2). Its experimental shift to 1274 cm^{-1} upon C8-deuteration (Fig. 4) supports well the calculated downshift to 1285 cm^{-1} (Table 3).

On the other hand, the present calculation mainly assigns the 1158 cm^{-1} Raman band to C4N9H and C8N9H angular bending coupled with bond-stretch motions (Table 2 and Fig. 3). Selective deuteration on labile hydrogens considerably modifies this mode, which actually vanishes in the spectra for the deuterated species (Fig. 5 and 6). It is again difficult to interpret this experimental observation on the basis of the assignment previously proposed (Florian et al. 1992).

700 cm^{-1} and below

The present calculations propose six in-plane vibrational modes in this spectral region. They are generally assigned to ring angular deformations coupled with ring stretching motions (Table 2). Under off-resonance conditions (Fig. 3), as well as in resonance with the 222 nm excitation wavelength, an intense band is observed at 638 cm^{-1}. Under the other two resonance conditions, two badly resolved RRS bands are observed at 650 and 638 cm^{-1}. These modes are highly affected by N-deuterations (Figs. 5 and 6, Table 6): they are calculated at 652 and 623 cm^{-1}, respectively (Table 2). Figure 7 shows that the latter mode bears a strong ring-breathing character. The importance of the purine breathing modes as DNA secondary structure conformational markers has been underlined in several experimental and theoretical investigations (Thamann et al. 1981; Ghomi et al. 1988). It should be stressed that, for the major purine nucleic bases, the most prominent

Table 3. Same as Table 2, but for $2NH_2A$-d1 (C8-deuterated derivative of $2NH_2A$). See also Fig. 4

Solution				Calc.	Assignments (PED)
R 488 nm	RRS 281 nm	RRS 257 nm	RRS 222 nm		
1704 (w)				1690	H-N6-H scissoring (21%), C2N2 (17%), C2N2H (9%), N1C6 (9%)
				1678	H-N2-H scissoring (47%), C2N2 (24%), C2N2H (21%)
				1664	H-N6-H scissoring (23%), C2N2 (16%), C6N6 (8%)
1611 (w)	1613 (m)	1612 (vs)	1612 (vs)	1617	N3C2 (30%), C2N1 (25%)
	1540 (w)			1544	C6C5 (24%), C5C4 (20%), C6N6 (12%)
1484 (w)	1485 (s)	1484 (s)	1484 (w)	1487	C8N7 (18%), C4N3 (13%), C5C4 (8%)
	1438 (vs)	1438 (w)	1439 (w)	1442	C4N9 (33%), C4N3 (25%), N3C4C5 (7%)
1374 (w)	1375 (sh)		1375 (sh)	1383	C8N7 (34%), C6N6 (12%)
1338 (s)	1338 (vs)	1339 (sh)	1340 (sh)	1345	N1C6 (33%), N7C5 (10%), C6C5 (10%), C5C6N6 (9%)
1274 (m)	1274 (vs)	1273 (w)	1275 (vs)	1285	N7C5 (31%), N1C6 (13%), C2N2 (10%)
1183 (sh)	1184 (sh)	1184 (w)		1214	N9C8 (57%), C4N3 (8%)
1147 (m)	1148 (m)	1148 (w)	1149 (w)	1147	C4N9H (26%), C6N6 (21%), C8N9H (17%)
	1082 (w)	1082 (w)		1069	C6N6 (18%), C2N2 (13%), C2N1 (13%), N9C8-D (8%), C6N6H (8%)
				1055	N9C8D (15%), C8N9H (12%), C4N9H (10%), C6N6 (10%), C8N7 (10%), C4N9 (8%)
981 (s)		982 (w)	981 (s)	1001	C4N9H (23%), C8N9H (15%)
948 (m)	950 (w)	948 (w)	949 (sh)	985	N3C2 (19%), C2N2H (16%), C4N9 (14%)
900 (w)	901 (w)	900 (w)		916	C2N2H (35%)
867 (w)				860	C2N2H (16%), C6N6H (13%), N9C8 (8%)
815 (w)	814 (w)		817 (w)	785	N7C8-D (26%), N9C8-D (18%), C8N9H (10%)
	648 (m)	649 (sh)		649	C5C6N6 (12%), C6N6 (10%), C2N1 (10%)
636 (vs)		637 (m)	636 (s)	616	C4N9 (20%), N3C4C5 (9%), C6C5 (8%)
547 (w)	546 (w)	546 (m)		567	C6C5 (12%), C2N1C6 (10%), C6N6H (9%), N3C2N2 (9%), N1C6N6 (9%)
501 (w)	502 (w)			501	C4N3C2 (11%), N1C6C5 (11%), C5C6N6 (10%), C4N3 (9%), N1C6 (8%), C2N2 (8%), N3C2N1 (8%)
				361	N3C2N2 (13%), N1C2N2 (12%), C6C5 (12%), N3C4N9 (11%), N7C5C6 (9%), C4N3 (8%)
				303	N1C6N6 (32%), C6N6H (16%), C5C6N6 (14%)

Table 4. Same as Table 2, but for $2NH_2A$-d5 (N2-, N6- and N9-deuterated derivative of $2NH_2A$). See also Fig. 5

Solution				Calc.	Assignments (PED)
R 488 nm	RRS 281 nm	RRS 257 nm	RRS 222 nm		
	1695 (s)			1671	C2N2 (39%), N3C2N1 (12%), C4N3 (8%)
1601 (w)	1602 (s)	1600 (vs)	1600 (vs)	1611	N3C2 (32%), C2N1 (29%)
				1543	C5C4 (22%), C6C5 (19%), C6N6 (14%)
	1514 (sh)	1515 (sh)	1516 (sh)	1501	C8N7 (24%), C6N6 (15%), N9C8H (10%)
1468 (w)	1468 (sh)	1466 (s)		1458	C4N3 (26%), C4N9 (18%)
	1430 (sh)			1425	N1C6 (20%), C6N6 (15%), C8N7 (11%), N9C8H (10%)
1359 (w)	1357 (sh)	1359 (sh)		1367	C6C5 (14%), N7C5 (12%), C8N7 (9%), C5C4 (8%)
1330 (s)	1331 (vs)	1330 (m)	1331 (s)	1318	D-N2-D scissoring (20%), N7C5 (21%), C2N2 (17%)
	1292 (s)	1291 (sh)		1283	N9C8H (33%), N7C8H (23%), C8N7 (14%)
				1276	N9C8 (18%), N7C8H (9%), D-N2-D scissoring (8%)
				1216	N9C8 (31%), N1C6 (13%), D-N6-D (10%)
1180 (w)	1178 (w)		1181 (w)	1182	D-N2-D scissoring (18%), N1C6 (16%), N9C8 (14%), N7C5 (13%)
1035 (w)		1034 (w)	1033 (w)	1059	C4N9 (28%), C6N6 (17%)
977 (w)				993	C2N1 (20%), N3C2 (17%), C6N6 (10%), D-N6-D scissoring (10%)
941 (w)	943 (w)	941 (w)	942 (w)	921	C6N6-D (12%), C5C6N6 (10%)
				896	C4N9-D (14%), N7C5 (11%), C2N2 (10%), N3C2N2 (8%)
		853 (w)	854 (w)	849	C4N9-D (10%), N7C8H (10%), C6N6-D (8%)
				740	C8N9-D (33%), C4N9-D (29%)
				725	C2N2-D (30%), C8N9-D (12%), C4N9-D (8%), C2N1C6 (8%)
613 (vs)	613 (m)	612 (m)	614 (s)	594	C6N6-D (16%), C6C5 (14%), N1C6 (9%)
				586	C6N6 (20%), C4N9 (8%)
		523 (w)		513	C6C5 (17%), C6N6-D (9%), N3C2N2 (8%)
491 (w)	490 (w)			478	N1C6C5 (12%), C4N3C2 (10%), N1C2N2 (9%)
				337	N3C2N2 (15%), N1C2N2 (14%), C6C5 (11%), N3C4N9 (10%), N7C5C6 (9%)
				263	N1C6N6 (31%), C6N6-D (27%), C5C6N6 (15%)

Table 5. Same as Table 2, but for $2NH_2A$-d6 (C8-, N2-, N6- and N9-deuterated derivative of $2NH_2A$). See also Fig. 6

Solution				Calc.	Assignments (PED)
R 488 nm	RRS 281 nm	RRS 257 nm	RRS 222 nm		
	1702 (w)			1671	C2N2 (39%), N3C2N1 (12%), C4N3 (8%)
1600 (w)	1602 (m)	1600 (vs)	1601 (vs)	1611	N3C2 (32%), C2N1 (29%)
1550 (w)	1550 (sh)			1539	C6C5 (20%), C5C4 (19%), C6N6 (18%)
1487 (sh)	1486 (sh)	1486 (m)	1485 (w)	1483	C4N3 (16%), C8N7 (15%), C6N6 (11%), C5C4 (9%)
1440 (m)	1440 (vs)	1442 (m)	1441 (w)	1453	C4N9 (16%), C4N3 (13%), N1C6 (12%), C6N6 (10%), C6C5 (8%)
	1407 (w)	1408 (sh)		1404	C8N7 (21%), C4N9 (13%), C4N3 (12%), N1C6 (12%)
1367 (sh)			1368 (w)	1362	C8N7 (21%), C6C5 (14%), N7C5 (11%), C6N6 (8%)
1323 (m)	1321 (m)	1322 (w)		1317	D-N2-D scissoring (21%), N7C5 (21%), C2N2 (17%)
1281 (s)	1282 (m)	1281 (m)	1280 (s)	1270	D-N6-D scissoring (12%), N7C5 (11%), C2N1 (9%), D-N2-D scissoring (8%)
	1214 (w)	1198 (w)		1214	N9C8 (33%), N1C6 (13%), D-N6-D scissoring (9%)
	1170 (w)			1177	N9C8 (23%), D-N2-D (16%), N1C6 (13%), N7C5 (10%)
				1060	C4N9 (28%), C6N6 (14%), C8N7 (9%)
		1034 (w)		1038	N9C8-D (36%), N7C8-D (15%)
979 (w)				991	C2N1 (20%), N3C2 (17%), D-N6-D scissoring (9%), C6N6 (8%)
936 (w)	938 (w)	936 (w)	937 (w)	912	C6N6-D (15%), C5C6N6 (11%), D-N6-D (8%)
	855 (sh)		854 (w)	888	N7C5 (17%), C2N2 (16%), C4N9-D (11%)
	824 (w)	823 (sh)		818	C4N9-D (19%), N7C8-D (15%), C8N9-D (9%), N9-C8-D (9%)
732 (w)				730	C2N2-D (43%), C2N1C6 (11%)
688 (sh)				707	C8N9-D (30%), C4N9-D (21%), N7C8-D (11%), N9C8-D (9%), C4N9 (9%)
612 (vs)	613 (s)	612 (s)	611 (s)	594	C6N6-D (16%), C6C5 (13%), N1C6 (9%), C2N1 (8%)
				583	C6N6 (17%), C4N9 (12%)
	518 (w)	519 (w)		509	C6C5 (16%), C6N6-D (10%), N3C2N2 (8%), N7C5C6 (8%)
497 (w)	496 (w)			477	N1C6C5 (12%), C4N3C2 (10%), N1C2N2 (8%)
				333	N3C2N2 (15%), N1C2N2 (14%), C6C5 (11%), N3C4N9 (10%), N7C5C6 (9%)
				262	N1C6N6 (31%), C6N6-D (28%), C5C6N6 (15%)

Table 6. Calculated frequencies of some of the most evident types of vibrational motions of $2NH_2A$ (pure species, see also Fig. 7) and corresponding observed and calculated shifts for the various deuterated species (in parentheses, following the order: $2NH_2A$-d1, $2NH_2A$-d5 and $2NH_2A$d6). For some of these modes, the rule of additivity of the spectral shifts (Alix 1975) on successive deuterations is qualitatively respected (see text)

Experimental (isotopic shifts)	Calculated (isotopic shifts)	Origin of the mode
1612 (0, −12, −12)	1617 (0, −6, −6)	Pyrimidine bond-stretchings
1508 (−23, +6, −21)	1507 (−20, −6, −24)	Imidazole bond-stretchings
1462 (−22, +4, −20)	1454 (−12, +4, −)	Pyrimidine + Imidazole bond-stretchings + exocyclic H-bendings
1402 (−17, +25, +6)	1400 (−25, +25, +4)	Imidazole + Pyrimidine bond-stretchings + exocyclic H-bendings
1349 (−9, +11, +19)	1348 (−3, +19, +14)	Imidazole + Pyrimidine bond-stretchings + exocyclic H-bendings
650 (−1, −36, −38)	652 (−3, −58, −58)	Base breathing mode
638 (−2, −, −)	623 (−7, −37, −40)	Base breathing mode

ring-breathing modes are located in the 700–500 cm^{-1} spectral region (Dhaouadi et al. 1993a, 1993b).

IV. Conclusion

In this paper, we attempted to give a plausible interpretation of the observed vibrational modes of $2NH_2A$ (under off- and on-resonance conditions) by a normal mode analysis using an empirical harmonic internal valence force field. The expansion of such a valence force field had been tested in our normal mode calculations on adenine (Dhaouadi et al. 1993a) and guanine nucleic bases (Dhaouadi et al. 1993b).

The purines are molecules of low point symmetry: their vibrational analysis is difficult since the number of force constants in a general valence force field far exceeds the number of measured wavenumbers. In order to reduce this problem and increase the number of experimental observables (band wavenumbers), the isotopic shifts upon selective deuterations should be taken into consideration: this has been done here. In the present calculations, the diagonal force constants of adenine (and those of guanine for the 2-amino group) have been transferred without modification. Some of the non-diagonal force constants have then been adjusted on the basis of the available Raman band shifts observed upon selective deuterations at various atomic sites. Our calculated wavenumbers are also in good agreement with those obtained experimentally in IR and Raman spectra of the pure $2NH_2A$ species in the polycrystalline phase (Florian et al. 1992). However, some of the normal mode assignments

(e.g. those corresponding to the observed 1612-, 1508- and 1158 cm^{-1} bands) proposed by Florian and coauthors within the framework of their ab initio force field are incompatible with the Raman band isotopic shifts experimentally observed in the present work. This is probably due to the fact that the corresponding scaling factors had been fitted by taking into account only the experimental data from the pure $2NH_2A$ species. Thus, it would be of interest to test these scaling factors on the basis of the experimental isotopic shifts presently reported. If this condition is fulfilled, the transferability of these factors might be recognized as valuable (see also Ghomi 1993).

The present work also shows that the band intensities of the Raman spectra of $2NH_2A$ and deuterated species are strongly dependent on the excitation wavelength. Excitations in the three apparent ultraviolet electronic absorption bands of the molecule are of interest for the forthcoming theoretical speculations which concern the determination of its excited state geometries.

Supplementary material available. Tables 2 to 5 with completed potential energy distribution (PED) down to 5% contributions can be obtained from M. Ghomi on request.

Acknowledgements. During his stay at the Institute Curie P. Mojzes was supported by a grant from the MICECO programme (French Foreign Office).

References

Alexeev G, Akimento NM, Volkova LI, Skuratovskii Y, Vorlickova M, Kypr J, Sagi J (1990) X form of poly(amino^{2}dA-dT): poly(amino^{2}dA-dT). Preliminary results of an X-ray fiber diffraction study. Studia Biophys 136:189–192

Alix AJP (1975) Théorie des perturbations générales des constantes moléculaires A, ζ^2, Σ, Γ_i, A_i: règles d'isotropie correspondant à la solution $(L^{-1} L^*) = \text{diag}$. Comptes Rendus Acad Sci Paris 281B:497–499

Borah B, Cohen JS, Howard FB, Miles HT (1985) Poly(d2NH_2A-dT): Two-dimensional NMR shows a B to A conversion in high salt. Biochemistry 24:7456–7462

Borah B, Howard FB, Miles HT, Cohen JS (1986) Conversion of poly(2-aminodeoxyadenylate-5-halodeoxyuridylate) from B to A forms in high salt. An NMR and circular dichroism study. Biochemistry 25:7464–7470

Coll M, Wang AHJ, van der Marel GA, van Boom JH, Rich A (1986) Crystal structure of a Z-DNA fragment containing thymine/2-aminoadenine base pairs. J Biomol Struct Dyn 4:157–172

Dhaouadi Z (1993) PhD dissertation, University Paris XIII

Dhaouadi Z, Ghomi M, Austin JC, Girling RB, Hester RE, Mojzes P, Chinsky L, Turpin PY, Coulombeau C, Jobic H, Tomkinson J (1993a) Vibrational motions of bases of Nucleic acids as revealed by neutron inelastic scattering and resonance Raman scattering. 1. Adenine and its deuterated species. J Phys Chem 97:1074–1084

Dhaouadi Z, Ghomi M, Coulombeau Ce, Coulombeau C, Jobic H, Mojzes P, Chinsky L, Turpin PY (1993b) The molecular force field of guanine and its deuterated species as determined from neutron inelastic scattering and resonance Raman measurements. Eur Biophys J 22:225–236

Florian J, Mojzes P, Stepanek J (1992) Scaled quantum mechanical force fields and vibrational spectra of solid-state nucleic acid constituents. 3. 2-aminoadenine. J Phys Chem 96:9278–9282

Gaffney BL, Marky LA, Jones RA (1982) The influence of purine 2-amino group on DNA conformation and stability. Synthesis and conformational analysis of d[T(amino A)]$_3$. Nucl Acids Res 10:4351–4361

Garriga P, Sagi J, Garcia-Quintana D, Manyosa J (1992) FT-IR spectroscopic study of the poly(amino2dA-dT) duplex in Mg^{2+} containing solutions and in films. J Biomol Struct Dyn 9:899–910

Ghomi M (1993) Reply to comments on "Vibrational motions of nucleic acids as revealed by neutron inelastic scattering and resonance Raman spectroscopy. 1. Adenine and its deuterated species". J Chem Phys 97:10890

Ghomi M, Letellier R, Taillandier E (1988) A critical review of nucleosidic vibration modes appearing in the 800–500 cm^{-1} spectral region, based on new harmonic dynamics calculations. Biopolymers 27:605–616

Gusoni M, Zerbi G (1968) Symmetry coordinates in molecular vibrations. J Mol Spectrosc 26:485–488

Howard FB, Chen CW, Cohen JS, Miles HT (1984) Poly(d2NH_2A-dT): Effect of 2-amino substituted on the B to Z transition. Biochem Biophys Res Commun 118:848–853

Kirnos MD, Khudyalov IY, Alexandrushkina NI, Vanyushin BF (1977) 2-aminoadenine is an adenine substituting for a base in S-2L cyanophage DNA. Nature 270:369–370

Khudyalov IY, Kirnos MD, Alexandrushkina NI, Vanyushin BF (1978) Cyanophage S-2L contains DNA with 2,6-diaminopurine substituted for adenine. Virology 88:8–18

Laigle A, Chinsky L, Turpin PY (1982) Resonance Raman spectroscopy of biomolecules in low concentrated solutions: signal/noise ratio improvement and background rejection by a fast Fourier transform treatment. Studia Biophys 89:99–105

Laigle A, Chinsky L, Turpin PY, Jolles B (1989) Kinetics of exchangeable protons in Z DNA: a UV resonance Raman study. Nucl Acids Res 17:2493–2502

Livramento J, Thomas GJ Jr (1974) Detection of hydrogen-deuterium exchange in purines by laser-Raman spectroscopy. Adenine 5′-monophosphate and polyriboadenylic acid. J Am Chem Soc 96:6529–6531

Majoube M (1985) Vibrational spectra of adenine and deuterium-substituted analogues. J Raman Spectrosc 16:98–110

Miskovsky P, Chinsky L, Laigle A, Turpin PY (1989) The Z conformation of poly(dA-dT) · poly(dA-dT) in solution as studied by ultraviolet resonance Raman spectroscopy. J Biomol Struct Dyn 7:623–637

Mojzes P, Chinsky L, Turpin PY, Miskovsky P (1992) Salt-induced conformational transition of poly(d2NH_2A-dT) studied by ultraviolet resonance spectroscopy. J Biomol Struct Dyn 10:181–194

Savitsky A, Golay MJ (1964) Smoothing and differentiation of data by simplified least square method. Annal Chem 36:1627–1638

Taboury JA, Adam S, Taillandier E, Neumann JM, Tranh-Dinh S, Langlois d'Estaintot B, Conti M, Igolen J (1984) The B to Z transition in two synthetic oligonucleotides: d(C-2amino-ACGCG) and d(m^{5}CGCAm^{5}CGTGCG) studied by IR, NMR and CD spectroscopies. Nucl Acids Res 122:6291–6305

Thamann TJ, Lord RC, Wang AHJ, Rich A (1981) The high salt form of poly(dG-dC) · poly(dG-dC) is left-handed Z-DNA: Raman spectra of crystal and solutions. Nucl Acids Res 20:5443–5457

Thomas GJ Jr, Livramento J (1975) Kinetics of hydrogen-deuterium exchange in adenosine 5′-monophosphate, adenosine 3′:5′ monophosphate and poly(riboadenylic acid) determined by laser-Raman spectroscopy. Biochemistry 14:5210–5218

Vorlickova M, Sagi G, Szabolcs A, Otvos L, Kypr J (1988) Conformation of the synthetic DNA poly(amino^{2}dA-dT) duplex in high-salt and aqueous alcohol solutions. Nucl Acids Res 16:279–289

Wilson EB, Decius JC, Cross PC (1955) Molecular vibrations. McGraw-Hill, New York